Polymer 51 (2010) 522–534

Contents lists available at ScienceDirect

Polymer

journal homepage: www.elsevier.com/locate/polymer

Correlation between polyethylene topology and melt flow instabilities by determining in-situ pressure fluctuations and applying advanced data analysis

Humberto Palza [a,b,*], Susana Filipe [a,1], Ingo F.C. Naue [a], Manfred Wilhelm [a]

[a] Institut für Technische Chemie und Polymerchemie, Karlsruhe Institute of Technology (KIT), Engesserstrasse 18, 76131 Karlsruhe, Germany
[b] Departamento de Ingenieria Quimica y Biotecnologia, Facultad de Ciencias Fisicas y Matematicas, Universidad de Chile and Centro para la Investigacion Interdisciplinaria Avanzada en Ciencia de los Materiales (CIMAT), Beauchef 861, Casilla 277, Santiago, Chile

ARTICLE INFO

Article history:
Received 13 July 2009
Received in revised form
10 November 2009
Accepted 23 November 2009
Available online 27 November 2009

Keywords:
Melt flow instabilities
Sharkskin
Polyolefins

ABSTRACT

Using three high sensitive pressure transducers located inside a slit-die of a capillary rheometer and applying a set of advanced mathematical tools to process the acquired time dependent pressure signals, we are able to detect in-situ pressure fluctuations associated with sharkskin instabilities. Other distortions, as spurt and gross melt fracture, can also be in-situ detected. This originates from a factor of 10^3 and 10^2 improvement in terms of time and pressure resolution achieved using the new set-up and data analysis that it will be described in detail in this article. Our approach quantifies the effect of polymer topology and shear rate on the characteristic frequency and amplitude of these pressure fluctuations inside the die. Depending on the polymer structure and the shear rate, different instabilities with large deviation in their main properties at melt-state, can be determined. Based on our results, a polymer-independent power law relationship between the characteristic frequency of the instability and the apparent shear stress has been found. Combining this new technique with the advanced mathematical analysis used, clear evidences concerning the origin and location of these instabilities, could be established. According to our analysis, the spurt instability starts in the entrance of the die and it propagates downstream while increasing its velocity along the die. This was confirmed by non-zero-time-lags in the cross-correlation function between the transducers located inside the slit-die. In case of sharkskin instability, pressure fluctuations inside the die indicate that its origin could also be already inside the die instead of being exclusively located at the die-exit region, as stated in earlier investigations.

1. Introduction

In polymer or food extrusion processes high throughput conditions are limited by melt flow instabilities which change the appearance and properties of the extrudate. Although these instabilities have been well known for several decades [1,2], their origins and mechanisms are still not clear, as each one has its own characteristics. There are three main instabilities depending on the shear rate and on the polymer properties, namely: sharkskin, spurt (or stick-slip), and gross melt fracture. For a controlled piston speed capillary rheometer, at low shear rates the polymer surface is smooth without any kind of perturbations. Increasing the shear rate, might lead to the appearance of sharkskin. Sharkskin consists of a periodic surface instability with both small amplitudes and high characteristic frequencies. The appearance of sharkskin depends on the material chosen [3] and it has been related with short chain branching in the polymer and low polydispersity. In the flow curve (a plot of the volume flux against the pressure) this instability is generally related with a change of the slope [2,4,5]. At higher shear rates some polymers show a spurt instability that is characterized by periodic smooth/rough regions in the extrudate, associated with large but slow pressure oscillations inside the barrel. A discontinuity in the flow curve is observed under these conditions and in pressure controlled rheometers a hysteresis appears [4,6]. Finally, at high shear rates more pronounced instabilities appear which are due to bulk phenomena, e.g. helicoidal defect, melt fracture, spiral defect, etc. These instabilities are called gross melt fracture. The common characteristic of the last instabilities seems to be its origin in the entrance of the die section due to turbulences or vortex formations in the barrel [2,7,8].

1.1. Sharkskin instability

The sharkskin instability seems to be related with a singularity in the flow dynamic of the polymer around the die-exit. There is large experimental evidence supporting this view [9–14]. It is well known

* Corresponding author. Departamento de Ingenieria Quimica y Biotecnologia, Facultad de Ciencias Fisicas y Matematicas, Universidad de Chile, Beauchef 850, Casilla 277, Santiago, Chile. Tel.: +56 2 978 40 85; fax: +56 2 699 10 84.
E-mail address: hpalza@ing.uchile.cl (H. Palza).
[1] Present address: Borealis Polyolefine GmbH, InnoTech Operational Support, Advanced Polymer Characterisation, Sankt Peter Strasse 25, 4021 Linz, Austria.

0032-3861/$ – see front matter © 2009 Elsevier Ltd. All rights reserved.
doi:10.1016/j.polymer.2009.11.050

that polymer molecules go through a dramatic change in their flow dynamic when they approach the die-exit. This is caused by a high velocity gradient at the die-exit where the flow evolves from e.g. a laminar shear flow with no-slip boundary condition, to a plug flow with free surface boundary condition. The singularity associated with the die-exit has been simulated and correlated with birefringence observations. Stress oscillations close to the exit, with a period similar to the formation of the instabilities, were found [9,11–14]. Based on the above observations several theories had been developed to explain the sharkskin instability, as for example those related with the melt rupture or cracking when the polymer leaves the die-exit [3,15], or theories based on the coil–stretch transition in a zone still inside the die, but very close to its exit [16,17].

The so-called crack theory assumes that due to the high elongational stresses at the die-exit, the polymer melt suffers a surface rupture (or cracking) since these stresses could have the same order of magnitude as the critical stress of melt rupture [11,12]. In this way, the instability was associated with the appearance of scratches and/or cracks located at the die-exit that become closer downstream due to some relaxation mechanism, producing an extrudate with the sharkskin appearance [18]. As pointed out by Wang et al. [16], no explicit explanation has ever been offered why this melt breakdown process appears periodic. Moreover, it was reported that some polymeric fluids with stress values in the die-exit higher than the onset stress for sharkskin instability are smooth when a slip surface is added in the die-exit. Therefore, the sharkskin instability does not occur because of the excess of melt deformation in the exit region [19]. This is an indication that the crack mechanism might not be plausible. Other theories are associated with an interfacial molecular instability. Wang et al. [4,20] developed a theory based on the coil–stretch transition concept in similarity to theories coming from the spurt instability [32]. Due to the exit singularity only chains that are close to the die-exit can have stresses high enough to undergo this transition. The oscillation in the stress level produces a small periodic perturbation of the extrudate swell, manifested in the form of sharkskin-like surface roughening. There are experimental findings that support this theory, for example the proportionality of the sharkskin wavelength with the overall chain relaxation time and/or the characteristic entanglement–disentanglement time. A second indication is the possibility to develop a master curve [17,21]. The theory of Wang et al. is also able to predict the periodical behavior of the sharkskin. Nevertheless, all these interpretations are in contradiction with theories based on the constitutive origin of the sharkskin inside the die (die-land region) [22–26].

1.2. Spurt instability

There is a general agreement that the origin of spurt instability is due to changes in the fluid-dynamic boundary conditions associated with a reversible transition from a non-slip (or stick) to a slip behavior at the die-wall [4,16,27]. In viscoelastic fluids the slip condition has been showed experimentally as a drastic increase in the velocity of the fluid at areas close to the wall when the polymer reaches a critical stress value [28–31]. The most accepted theory to understand this process was developed by Brochard and de Gennes [32] based on the reptation model. The effective diameter (e.g. radius of gyration) of one chain adsorbed at the wall decreases inversely proportional to the velocity of the surrounded or bulked polymers (stretch process). At a certain velocity, the diameter of the adsorbed polymer will be lower than the diameter necessary for entanglements. Under these conditions, the frictional forces decrease and the effective slippage-length, defined as the imaginary distance from the wall where the velocity of the fluid is zero, increases drastically as the chain disentangle from the bulk. In this new state the chain at the wall will relax (coil process) and it will entangle again with the bulk chains, repeating the whole process. The reversible coil–stretch transition theory explains why this instability is observed mainly in polyethylenes, since these polymers have both, smaller entanglement molecular weights and higher average molecular weights than other commercial polymers [33]. Macroscopically, by means of a mass balance inside the barrel, the main characteristics of this instability can be numerically simulated [34–36]. At non-slip conditions, the flow associated with the movement of the piston inside the barrel is higher than the extrudate flow, or flow inside the die, therefore a compression cycle develops. If the slip condition occurs inside the die, the flow associated with the piston will be lower than the flow of the polymer within the die. Therefore a decompression process occurs until the system relaxes and the non-slip condition is valid again. In this way, it is possible to understand the pressure oscillation and its dependence on the barrel volume due to the compressibility of the polymer. One of the problems with theories based on slip processes is the assumption of a non-slip condition for models that are able to predict the spurt instability from constitutive equations [2,37,38]. This is in clear contrast with the above-mentioned experimental findings. Independently of the origin of the spurt instability, it is assumed that the process that causes the instability is simultaneous and spatially homogeneous along the die surface. Moreover, mathematical models predict only the pressure evolution inside the barrel. Therefore, a more detailed characterization about the dynamic of this instability inside the die is needed and it is one of the main goals within this article.

As described above, it is clear that more advanced experimental setups and data analysis are necessary to gain a better understanding of the behavior of melt flow instabilities. The preliminary work done within our group on the development of a non-conventional set-up for the evaluation of melt flow instabilities ensured a significant improvement in terms of both time and pressure resolution, by a factor of 10^3 and 10^2, respectively [39,40]. It is relevant to point out that, such improvement led to the achievement of a time resolution Δt of around 1 ms, in combination with a pressure resolution ΔP of 5 mbar. Such development proved to be crucial to detect and characterize instabilities, which would not be detectable solely by the use of conventional setups [39,40]. The preliminary work done on this improved tool allowed the understanding of the effects of uniaxial extensional properties on the onset of melt flow instabilities (most specifically, stick-slip), for industrial broad molecular weight distributed polyethylenes [40].

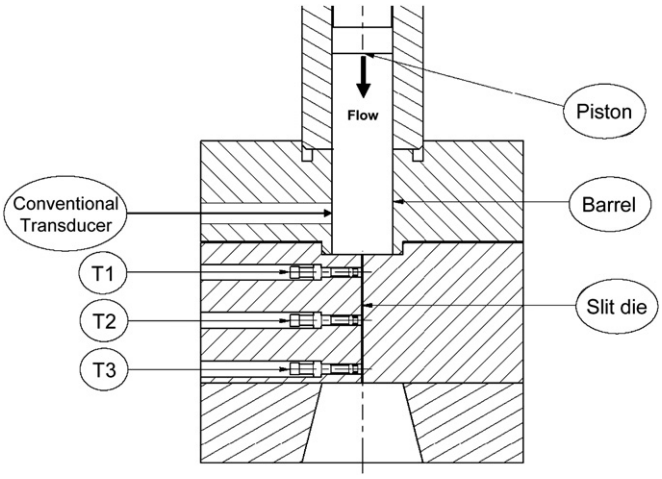

Fig. 1. Technical drawing of the home-made slit-die designed with three high sensitive pressure transducers inside the slit ($0.3 \times 3 \times 30$ mm^3), labeled as T1, T2 and T3.

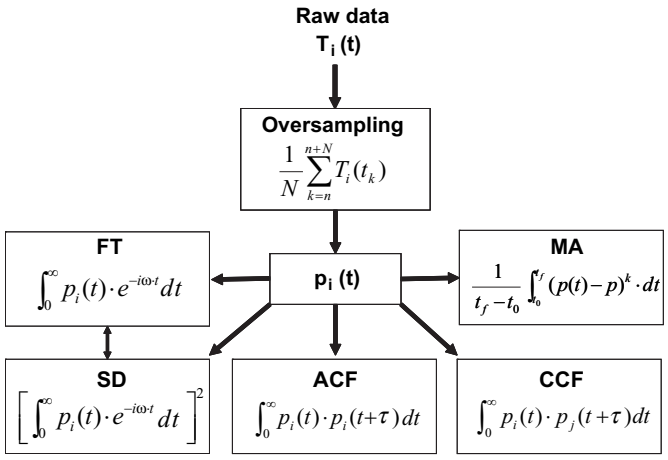

Scheme 1. Summary of the mathematical tools used to analyze the data from our new set-up. The subscript *i* refers to the different transducers. SD, spectral density; ACF, auto-correlation function; FT, Fourier transform; CCF, cross-correlation function; MA, moment analysis.

Additionally, it was possible to elucidate the correlation of the onset of melt flow instabilities with material structural properties (molecular weight – Mw, molecular weight distribution – MWD and topology) for industrial polyethylenes possessing broad MWD.

The main goal of the present publication is to enlarge the study described above to other materials and to characterize in-situ the effect of polymer topology and shear rate on the pressure fluctuations, as well as the characteristic frequencies of melt instabilities. The work here presented combines the application of the set-up developed by Filipe et al. [39,40], that makes use of high sensitive pressure transducers located inside the die (see Fig. 1), with a new advanced mathematical framework to process the acquired time dependent pressure signals (see Scheme 1). Our analysis will give a new perspective of the main parameters that characterize melt flow instabilities correlating them with material structural properties such as Mw, MWD and topology. Moreover, by measuring the cross-correlation function for the pressure signals coming from the transducers located along the die, we can evaluate the dynamic of these phenomena.

The outlook of our novel approach is to generate an "intelligent" extruder able to detect in-situ the onset of melt instabilities and to change the flow conditions to avoid, e.g. sharkskin. In this way, the extruder itself will be able, by means of a "loop" control system, to avoid extrudate distortions.

2. Experimental

To study the whole range of instabilities, four commercial polyethylenes of different topologies were chosen. PE-L is a linear high-density polyethylene and PE-LCB is a long-chain branching low-density polyethylene, both from Lyondel BASELL. Two ethylene/1-octene copolymers from Dow with a short chain branching (SCB) incorporation of 7 (PE-7SCB) and 13 mol% (PE-13SCB) were also studied. The melt flow rates (190 °C/2.16 kg) are: 0.10, 0.75, 3.0 and 5.0 g/10 min for samples PE-L, PE-LCB, PE-7SCB and PE-13SCB, respectively. The details of the molecular weight, topology, and melting points of the samples are given in Table 1.

Capillary flow measurements were carried out on a GÖTTFERT Rheo-tester 2000 capillary rheometer at 190 °C for PE-L and PE-LCB samples and 140 °C for PE-7SCB and PE-13SCB samples. These temperatures were chosen to avoid differences in melt-state properties due to the different topologies and molecular weights of the four polyethylenes. Both the shear stress and the shear rate were measured without any correction (e.g. Bagley or Rabinowitch). The slit-die used in this work is home-made and non-conventional (see Fig. 1). It was specifically designed in order to allow the evaluation of the pressure fluctuations at three different locations along its length at 3, 15 and 27 mm and named T1, T2 and T3, respectively [39,40]. The total die length is 30 mm with a cross section of 3.0 mm × 0.3 mm. The evaluation of the pressure was done via fast acquisition piezoelectric pressure transducers (model 6812B, from KISTLER, Switzerland). The use of these fast response transducers, coupled with oversampling techniques [41–43], allowed a substantial improvement by a factor of 10^3 and 10^2 in terms of both time and pressure resolutions when compared with a conventional set-up [39,40]. The limiting time resolution Δt is typically 1 ms after oversampling and 5 mbar for the pressure resolution ΔP in our set-up [39,40]. The collected pressure data were further treated using statistical analysis. After oversampling, Fourier analysis is performed on the time dependent pressure data, and the observed peaks at the frequency-domain are located at frequencies that are the inverse of the related time scale of the instability. More details about this set-up are found in Refs [39] and [40].

The viscoelastic properties of the samples were obtained in an ARES rheometer from TA Instruments using a 25 mm diameter parallel plate at 140 and 190 °C. Oscillatory shear experiments in the linear regime were conducted in a frequency range from 10^{-2}–10^2 rad s^{-1}, under nitrogen atmosphere.

3. Details of the data analysis

As it will be shown below, our method allows detecting a dynamic range at 4–5 decades in the pressure signals (see for example Fig. 10). Therefore, fluctuations as small as 0.01% with respect to the main value can still be quantified. This is only possible by using our new set-up in combination with advanced mathematical tools in order to improve the pressure signals and its analysis. In this chapter we would like to introduce the main concepts behind the mathematical analysis used in this contribution. This mathematical framework is summarized in Scheme 1 and Fig. 2.

Table 1
Main characteristics of the polyethylenes studied.

Sample	Estimated topology	M_w (kg/mol)	M_n (kg/mol)	Melting point (°C)	Relaxation time[d] (s)	Onset instability		Main instability
						Shear rate (1/s)	Shear stress (MPa)	
PE-L	Linear	193	20	128.4	0.2	140	0.22	Spurt
PE-LCB	Long chain branching[a]	186	20	114.4	0.32	< 100	< 0.1	Gross Melt Fracture
PE-7SCB	Short chain branching[b]	100	45	99.8	< 0.01	155	0.25	Sharkskin
PE-13SCB	Short chain branching[c]	85	37	64.2	< 0.01	65	0.11	Sharkskin

[a] 3 LCB/1000 CH_2.
[b] 7% mol SCB.
[c] 13% SCB.
[d] Estimated from the crossover point between the elastic and viscous moduli in a frequency sweep test at 190 °C.

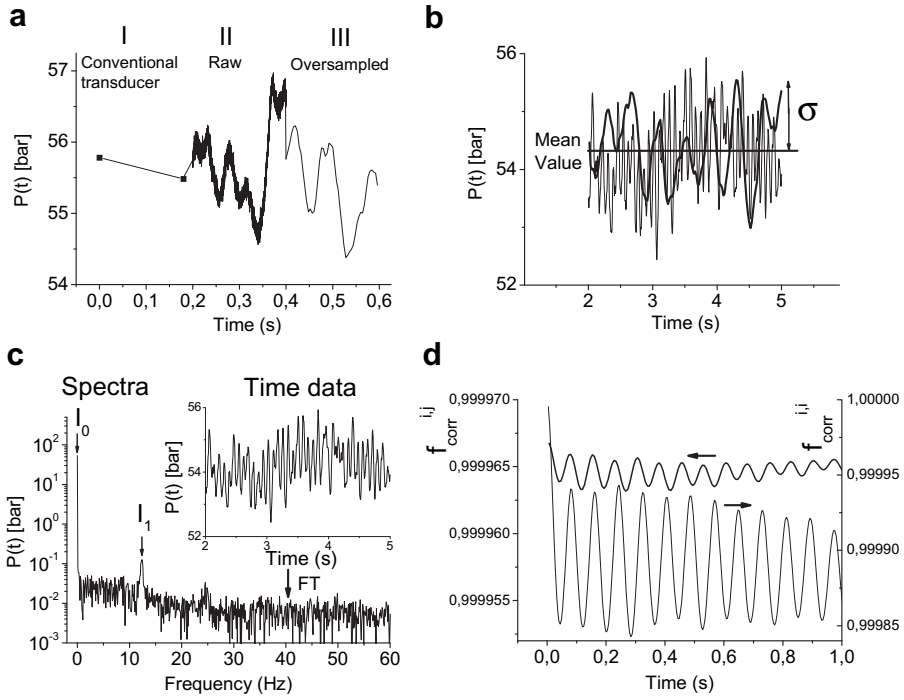

Fig. 2. Examples of the mathematical framework used in our data analysis for a representative pressure fluctuation from a gross melt fracture instability. (a) Region I, original data obtained by a conventional transducer, typical scan rate of 4×10^0 point/s; Region II, oversampled data taken with a scan rate of 3.3×10^4; Region III, data after oversampling technique with a final scan rate of 2.5×10^2. (b) Moment analysis for data after oversampling method, showing the first (mean value) and the square root of the second (standard deviation) moments of the pressure fluctuation. It is presented two different examples but with the same results from the moment analysis. (c) Fourier transform (FT) spectra of the time-data pressure fluctuation. (d) Auto-correlation function ($f_{corr}^{i,i}$) for T1 and cross-correlation function for T1 and T2 ($f_{corr}^{i,j}$). In this particular case the pressure fluctuations associated with T1 and T2 are correlated and in phase as at zero time-lag the function shows a maximum.

3.1. Oversampling

Oversampling is a method that allows increasing the signal to noise ratio [41–44]. The idea is to acquire the pressure data at the highest possible acquisition rate and therefore the raw data are "oversampled" (see region II in Fig. 2a). After that, the raw time data are truncated "on the fly" by means of a so-called "boxcar" average over a certain amount of raw data points. The average is over a fixed number of data points (N) between t and $t+\Delta t$ that results in a single data point at $t+0.5\Delta t$:

$$p(\tau_n) = p(t_n + 0.5\Delta t) = \frac{1}{N}\sum_{k=n}^{n+N} T(t_k) \tag{1}$$

where $T(t)$ represent the original raw data from the pressure transducer at time t, and $p(\tau)$ is the pressure signal after applying the oversampling method (see region III in Fig. 2a). Each of these new values has an inherently lower relative stochastic noise level due to the applied averaging procedure. The application of the boxcar average to the raw time data results in a new time domain data points with a strongly reduced random noise. For a pure stochastic noise, a signal to noise (S/N) improvement by $N^{1/2}$ can be achieved if N time data points are pre-averaged, with typical values of N in the range of 10–1000.

3.2. Moment analysis

The moment analysis (MA) is the first method normally used to characterize time dependent experimental data. Using concepts coming from statistical analysis, it gives information about the general distribution of a random variable, in this case the pressure signal [45]. The definition of the k-moment is as follows:

$$m_k = \frac{1}{t_f - t_0}\int_{t_0}^{t_f} (p(t) - \overline{p})^k \mathrm{d}t \tag{2}$$

$$\overline{p} = \frac{1}{t_f - t_0}\int_{t_0}^{t_f} p(t)\mathrm{d}t \tag{3}$$

where m_k is the kth moment of the pressure and $\overline{p}$ represent its mean value; $p(t)$ is the time dependent pressure signal. From Eq. (3) it is observed that evaluating the first moment around zero instead of around $\overline{p}$, we obtain the mean (or expected) value of the pressure (see Fig. 2b). The second moment is the variance of the function and its positive square root is the standard deviation (see Fig. 2b). The third moment is related with the asymmetry of the time dependent signal. Despite the utility of the moment analysis, it looses relevant characteristics from the dynamic of the experimental data. In particular, this method is inherently not able to represent the characteristic time scale of the analyzed function. One example of this restriction is shown in Fig. 2b.

3.3. Fourier analysis

A Fourier transform (FT) is a mathematical method to quantify the inherent periodic contributions from a time dependent signal. It displays their amplitudes and phases as a function of the frequencies [42–45]. In this way, a complete characterization of experimental periodic functions without lose of any information is achieved. The FT of any real or complex time signal, in our case the pressure $p(t)$, or frequency dependent spectrum $P(\omega)$, is usually defined in the following way:

$$P(\omega) = \frac{1}{\sqrt{2\pi}} \int_0^{+\infty} p(t) e^{-i\omega t}\, dt \quad (4)$$

$$p(t) = \frac{1}{\sqrt{2\pi}} \int_0^{+\infty} P(\omega) e^{+i\omega t}\, d\omega \quad (5)$$

where $\omega = 2\pi f$, with f representing the frequency. From Eqs. (4) and (5), it is possible to define the spectral density function $D_P(\omega)$:

$$D_P(\omega) = \left[\int_0^{+\infty} p(t) e^{-i\omega t}\, dt \right]^2 \quad (6)$$

In general the Fourier transform is an invertible, linear, and complex mathematical operation. The Fourier spectra $P(\omega)$ have non-zero values only at frequencies $\omega/2\pi$ that are present within the original time dependent function (see Fig. 2c). By using FT analysis it is possible to find parameters that quantify the time dependent signal. Therefore, under melt instability conditions the time dependent pressure data can be described as a sum of different harmonic contributions:

$$p(t) = \overline{p} + \sum_{i \geq 1} I_i \cos(\omega_i t + \phi_i) \quad (7)$$

where $\overline{p}$ is the pressure mean value; $\omega_i/2\pi$, φ_i and I_i are the related characteristic frequencies, phases, and amplitudes of the pressure fluctuation as quantified from the Fourier analysis of the processed signals. It is assumed that all the information related with the melt instability is included in these parameters: ω_i, φ_i and I_i, since an FT is an invertible mathematical operation. In the Fourier spectra the intensity at $\omega/2\pi = 0$ is the mean pressure value $\overline{p}$ of the signal.

A measure of the relative pressure fluctuation (RPF) could be I_1/I_0, where I_0 represent the peak value at 0 Hz that is related with $\overline{p}$, and I_1 represent the first main peak value at a frequency higher than 0 Hz ($i = 1$ in Eq. (7)), both values referred to the same transducer (see Fig. 2c). The last is a simplification as the RPF is associated with all the harmonics present in the signal, function usually called distortion factor. Therefore, it is assumed:

$$\mathrm{RPF} = \frac{\sum_{i \geq 1} I_i}{I_0} \approx \frac{I_1}{I_0} \quad (8)$$

since $I_1 > I_n$ for $n > 1$ [42].

3.4. Correlation functions, auto- and crosscorrelation

The time evolution of a pressure signal can be characterized by the auto-correlation function as defined by [45]:

$$f_{\mathrm{corr}}^{i,i}(\tau) \propto \int_0^{\infty} p_i(\tau) p_i(t+\tau) dt \quad (9)$$

where i represents the transducer that is studied. The auto-correlation function shows the time correlation of the same fluctuating physical quantity at different times. It gives information about the "memory" and time persistency of a signal and it quantifies itself similarity. The characteristic time at which the auto-correlation function approaches $1/e$ is called the correlation time. The auto-correlation function of a periodic signal is also a periodic function with the same characteristic frequencies (Fig. 2d). In our analysis, this function is relevant as the noise does not correlate.

To study the dynamic of the instability along the die, the cross-correlation function of the pressure transducer can be used for quantifying the correlation of the time dependent pressure signals coming from the different transducers ($i \neq j$) [45]:

$$f_{\mathrm{corr}}^{i,j}(\tau) \propto \int_0^{\infty} p_i(\tau) p_j(t+\tau) dt \quad (10)$$

The subscripts i and j represent the different transducers along the die. For periodic functions the cross-correlation function is also periodic and its value at zero-time-lag is related to the time/phase lag between them. If there is a maximum in the cross-correlation function at zero-time-lag the functions are highly correlated and in-phase, therefore the events could be assumed to happen simultaneously (see Fig. 2d). Otherwise, the functions are out of phase and the related shift can be quantified. Similar information is possible by analyzing the difference in phase coming from the Fourier transform between the transducers ($\varphi_i - \varphi_j$, from Eq. (7)), as it will be discussed below.

3.5. Turbulence analysis and chaos

Although it is not used in this contribution, we want to highlight that mathematical tools originated from the chaos analysis are possible to apply. This kind of analysis will further extend and complement our knowledge about polymer melt flow instabilities. As it will be shown below, some samples present instabilities with pressure fluctuations that appear irregular at time and therefore they can be related with a massive non-linear behavior of the system under these conditions [46]. Methods as the FT are not viable anymore for these signals and become extremely complex. In these cases, the chaotic behavior could be checked by, e.g., the maximum Lyapunov exponent that gives a measure of the divergence of two nearby trajectories belonging to a deterministic attractor. If this parameter is higher than 0 the attractor is chaotic [46]. Therefore, data from our highly sensitive set-up could also open a new perspective about non-linear fluid-dynamic systems at very high shear rates.

4. Results

4.1. Flow curve analysis

Fig. 3 displays the storage and loss moduli for the four samples as determined via oscillatory shear in the linear regime. The characteristic relaxation time as the inverse of the crossover point was determined (Table 1). The differences between PE-L/PE-LCB and PE-7SCB/PE-13SCB samples are obvious. In particular, PE-L shows the highest elastic behavior at low frequencies due to the long-chain branching and no evidence of the terminal zone is detected [47]. At high frequencies these differences tend to disappear. Fig. 4 shows the flow curves for all the samples measured in the capillary rheometer. The sample PE-L has a singularity at a shear rate of 140 s^{-1} that is a typical behavior for high-density polyethylenes [48]. PE-LCB does not show any significant change in its flow curve in the range studied, indicating the strong influence of the amount of long-chain branching on the flow curve of the polymer. Samples with short-chain branching present a smooth change in the slope of the flow curves at shear rates of 155 and 65 s^{-1} for PE-7SCB and PE-13SCB, respectively. The change in the slope is associated with the sharkskin instabilities (see below). Increasing the amount of short chain branching, both the shear strain and shear stress necessary for the onset of this instability tend to decrease. This tendency was related with the lower entanglement density (or rubbery plateau modulus) of polymers with higher amount of short chain branching [49].

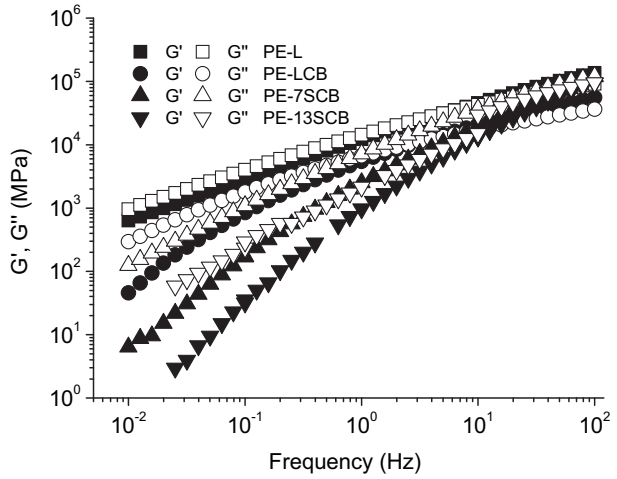

Fig. 3. Elastic (G') and viscous (G'') moduli for the different samples studied. Temperatures of 190 °C for PE-L and PE-LCB samples, and 140 °C for PE-7SCB and PE-13SCB samples.

The specific melt instabilities that these polymers develop are related with the different behavior found in their flow curves [21,50]. Using our new in-situ method inside the die, reliable quantification of the main parameters that characterize these phenomena is possible. Therefore, the relation between polymer topology and its melt instability can be analyzed directly inside the die.

4.2. Effect of the long-chain branching

In order to analyze the effect of the long-chain branching, first the PE-L sample is studied as it is a linear polymer with low amount of branching. An example of the pressure oscillations at the T1, T2 and T3 transducers for this sample is presented in Fig. 5 at an apparent shear rate of 283 s^{-1}. The original pressure signals after oversampling (Fig. 5a), the pressure normalized by its mean value (Fig. 5b), and the respective Fourier analysis (Fig. 5c), are shown. Large but slow pressure fluctuations are detected (around 10% with respect to the mean value). At these conditions PE-L develops spurt instability as similar pressure oscillations are observed by the conventional transducer located in the barrel (not shown here). These massive distortions are related with the appearance of alternate smooth/rough regions in the extrudate. In this way, the singularity observed for this sample in the flow curve (Fig. 4) is due to the

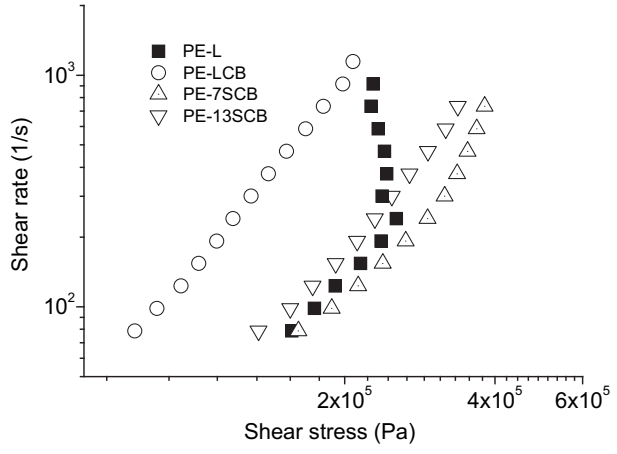

Fig. 4. Flow curves for the different samples. Temperatures of 190 °C for PE-L and PE-LCB and 140 °C for PE-7SCB and PE-13SCB.

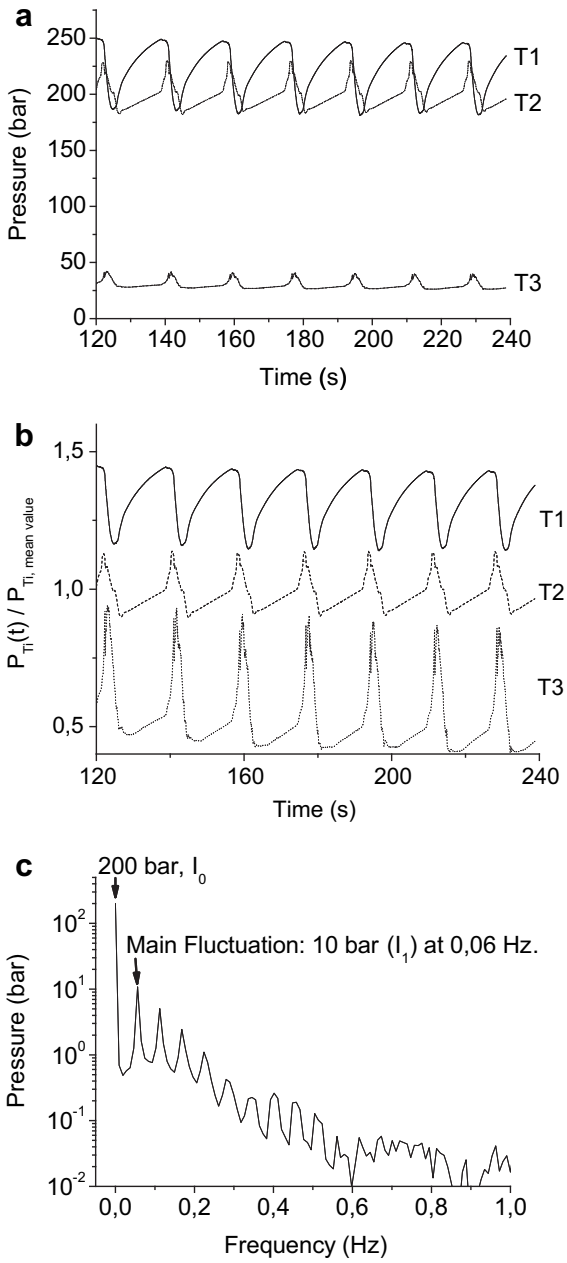

Fig. 5. Data from PE-L sample at a shear rate of 283 s^{-1} where the spurt instability develops. (a) Pressure signals detected inside the die. (b) The associated normalized pressure fluctuations (curves are shifted by ±0.2 in the vertical axes for a better representation). The subscript Ti represents the different transducers. (c) The respective Fourier transform for the T1 signal.

development of this instability. The pressure oscillations measured by the piezo-electric transducers have the same frequencies than those detected in the conventional pressure transducer, and these fluctuations are around 0.05 Hz. The signal from T1 shows the same behavior that the signal from the conventional transducer, both having the same dynamic in the pressure oscillation: asymptotic increases in pressure (stick process) followed by a fast and drastic decrease in it (slip process), as it is well known for this kind of instability. In the Fourier analysis of the T1 signal is not only possible to quantify the peak related with the mean value of the pressure (at 0 Hz) and the main peak associated with the pressure oscillation (at 0.05 Hz) but also other peaks that are due to the presence of higher harmonics of the pressure oscillations (see Eq. (7)) [42]. It is also

possible to observe that T2 has the same periodic behavior as at T3 although the shape being different from T1. At the beginning of the instability, in T2 (or T3) the pressure drastically increases instead of decreases as in T1. After that, a sharp and strong decrease is observed. Furthermore, as we proceed more along the die length one can observe both a sharpening of the pressure maximum (T2 and T3), which is as stronger as we approach more the die exit, and a broadening of the pressure minimum. Assuming that the slip develops first in some area upstream of T2 and it propagates downstream later on as an "avalanche", it is likely to understand this behavior. In the very beginning of the slip phenomenon the flow passing by the area around T2 will be higher than the flow that goes out, so a compression must occur with increasing pressure, similar as in the T3 region. After that, the slip phenomenon propagates downstream, so the pressure in these areas will go-down as it is observed in our data. To explain the above mentioned we can use two methodologies: the first one is the analysis of the change in the flow-pressure due to the instability by means of the integral form of the Bernoulli theorem based on an energy balance in the system [51]:

$$-\int_S p\cdot\vec{u}\cdot\vec{n}\cdot dS=\int_V(\bar{\bar{T}}:\bar{\bar{D}})\cdot dV-\int_S(\bar{\bar{T}}\cdot\vec{n})\cdot\vec{u}\cdot dS-\int_V p\cdot div(\vec{u})\cdot dV \tag{11}$$

where p is the pressure, $\bar{\bar{T}}$ is the extra stress tensor, $\bar{\bar{D}}$ is the rate of deformation tensor, $\vec{u}$ represents the velocity field, $\vec{n}$ is the normal vector directed outside of the flow domain V, and S is the surface of the flow domain. Analyzing the changes in the velocity of the fluid by means of this equation is possible to qualitatively understand the pressure drops as the instability propagates inside T2 or T3 [51]. The second methodology is based on a constitutive equation for viscoelastic materials together with the Mooney correction related with a decrease of the shear rate at the wall when the slip occurs. Due to the complexity associated with Eq. (11), the first approach is not easy to compute numerically. Therefore, we chose the second approach since it allows a semi-quantitative agreement of our findings in a more direct way. We applied the Giesekus model, which is a constitutive equation with three parameters predicting the non-linear responses of the stresses. Using the notation from Bird et al. the Giesekus model is based on the following equations [52]:

$$\bar{\bar{\tau}}+\lambda_1\cdot\bar{\bar{\tau}}_{(1)}-\alpha\cdot\frac{\lambda_1}{\eta_p}\{\bar{\bar{\tau}}\cdot\bar{\bar{\tau}}\}\;=\;-\eta\cdot\bar{\bar{\dot{\gamma}}} \tag{12}$$

where:

$$\bar{\bar{\tau}}_{(1)}\;=\;\frac{D\bar{\bar{\tau}}}{Dt}-\left\{(\nabla\vec{v}_k)^t\cdot\bar{\bar{\tau}}+\bar{\bar{\tau}}\cdot(\nabla\vec{v}_k)\right\} \tag{13}$$

$$\frac{D}{Dt}\tau\;=\;\frac{\partial}{\partial t}\tau+\{\vec{v}_k\cdot\nabla\tau\} \tag{14}$$

The non-linear parameter α is related with anisotropic Brownian motions or anisotropic hydrodynamic drag on the constituent polymer molecules and it can have values between 0 and 1. The components $\bar{\bar{\dot{\gamma}}}$ and $\bar{\bar{\tau}}$ are associated with the shear rate and shear stress tensors, and $\vec{v}_k$ is the component of fluid velocity vector. The parameter η is the zero-shear-rate viscosity and λ is the relaxation time. The equations are solved numerically using Cartesians coordinates assuming infinite walls and they were evaluated at the wall in a point equivalent to the position for T2. It is assumed that any change in the hydrodynamic boundary conditions are reflected instantly in the shear rate at the wall and the time evolution of the stress is analyzed. It is further assumed that the piston movement forces the system at a steady shear rate. When the slip first develops upstream T2, the shear rate increases because of the higher mass flow that come-in. After that, the slip propagates downstream reaching the T2 area and the shear rate drops as it could be predicted by the Mooney correction [34]. A linear relation between τ_{zx} (evaluated at the wall) and the pressure is assumed. The lasts hypothesis simplifies the system and allows us to give a first approximation of our findings. Based on the last equations and assumptions, the data in Fig. 6 are obtained. The mathematical simulation represents properly the dynamic of the system and gives a reasonable quantification of the relative pressure fluctuation (around 10%). Therefore, it is possible to conclude that with these very simple approximations we are able to gain a semi-quantitative explanation of our findings for T2 (the same occurs for T3). The simulation supports the concept that the instability could be generated in some area upstream T2 and it further develops downstream.

The propagation of the spurt instability can be further confirmed by the cross-correlation function between the different pressure signals from T1, T2, and T3. From Eq. (10) the cross-correlation between the pressure fluctuations coming from the different transducers is experimentally quantified. Fig. 7 displays the cross-correlation of T1–T2 and T2–T3. Non-zero-time-lags in the maximum of the correlation functions for T1–T2 and T2–T3 (at 2.3 s and 0.95 s, respectively) are found, confirming the downstream-propagation of this instability as an "avalanche". Moreover, it is possible to estimate – to our knowledge for the first time – the velocity of the propagation knowing the distance between the transducers. The instability accelerates along the die from about 5–13 mm/s between the T1–T2 and the T2–T3 sections. These time-lags are additionally confirmed by analyzing the phase difference of the pressure signals (see Eq. (7)) measured by the Fourier analysis. The propagation velocities have the same order of magnitude as the average velocity of the fluid in the capillary ($\approx$10 mm/s), estimated assuming the non-slip condition at the die-slit.

A different behavior is observed for the PE-L sample at 2047 s^{-1} (Fig. 8). The pressure fluctuation decreases one order of magnitude being around 1% relative to its mean value. The time evolution of the fluctuation also changes and periodicities around 0.1 s are detected. Noteworthy, these fast and small fluctuations cannot be detected by the conventional transducer and they do not have the characteristics of the spurt instability. From Fig. 8b we can measure

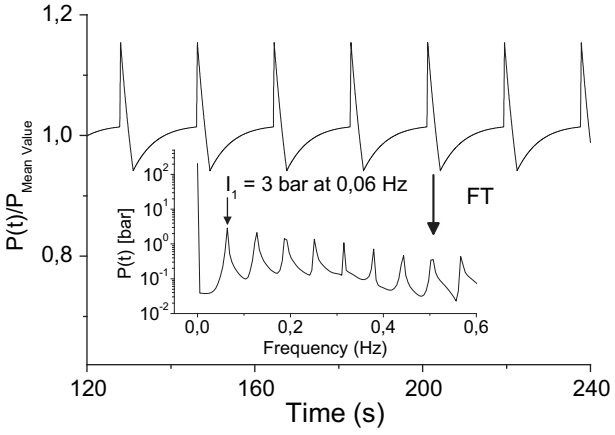

Fig. 6. Numerical simulation of the normalized pressure fluctuation using the Giesekus constitutive equation (see text for details). The parameters are: $\eta = 100$ Pa s, $\alpha = 0.2$, and $\lambda = 6.0$ s. The shear rate is assumed to be 0.1 s^{-1} when the flow is piston-controlled, 0.4 s^{-1} when the mass flow upstream is higher than downstream (beginning of the instability), and 0.05 s^{-1} when the slip propagates. See text for details about the simplifications done. Inside the Figure the respective Fourier spectra is shown.

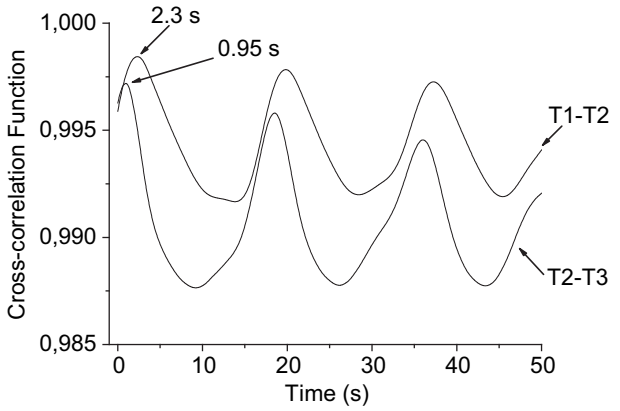

Fig. 7. Cross-correlation function between the different transducers for sample PE-L at a shear rate of 283 s^{-1} where a spurt instability is developed. See Eq. (10) for details.

the average characteristic frequency which is around 27 Hz. By means of an optical microscopy the characteristic length of this instability in the solid extrudate was measured (1.8 mm in this particular case). Knowing the mean velocity of the extrudate coming-out from the slit-die, the characteristic frequency of the instability is estimated to be around 17 Hz. The frequencies have approximately similar values and the difference can be explained by changes in the polymer associated with the transition when the material changes from lamellar flow inside the die towards plug flow at the exit of the die. Further complication can arise from crystallization, swelling phenomena, normal forces, gravity, etc. Therefore, the high sensitivity piezo-electric transducers, together with our novel data analysis, are able to detect pressure oscillations related with the main characteristics of the distortions from the extrudate at high shear rates. Under these conditions the extrudate presents a continuous wavy bulk distortion associated with a gross melt fracture (see section *Effect of the die-entrance angle* for details). The pressure signals along the die are completely correlated and in-phase as the maximum in the cross-correlation function is at zero-time-lag, independently of the transducers that are analyzed. The last finding could mean that the gross melt fracture originates in the entrance of the barrel producing some kind of fluctuating plug flow inside the die.

By investigating the PE-LCB sample it is possible to analyze the effect of the long-chain branching towards the pressure fluctuations inside the die. Fig. 9 displays the normalized pressure signals from T1 and T2 for this sample at a shear rate of 787 s^{-1} together with the Fourier analysis for T1. From Fig. 9b it is clear that the behavior of the instabilities coming from PE-LCB is completely different and a broad peak around 4 Hz instead of a very sharp-defined peak appears (compare Figs. 8 and 9). Furthermore, the extrudate presents a continuous wavy bulk distortion associated with a gross melt fracture within the whole range of shear rates

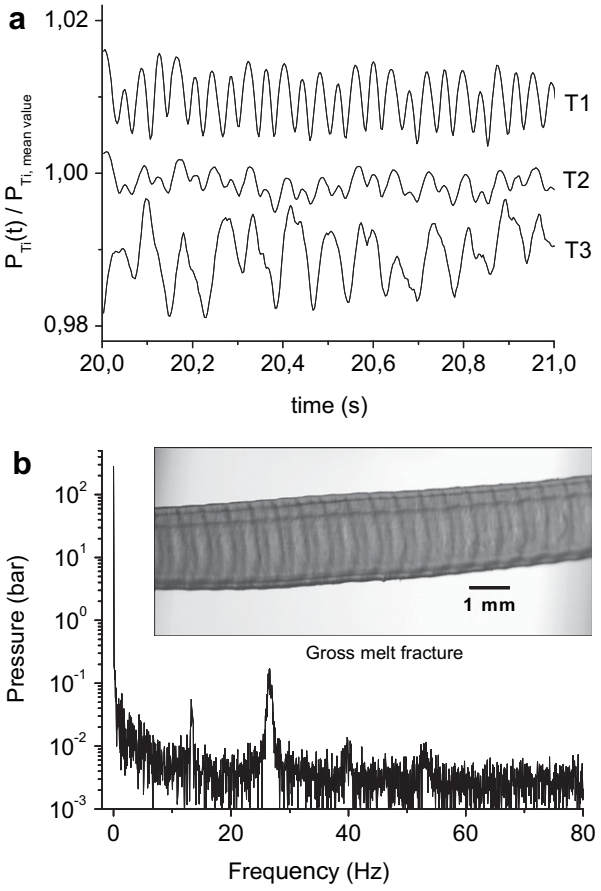

Fig. 8. Pressure fluctuations and related spectra for PE-L sample at a shear rate of 2047 s^{-1} where a gross melt fracture instability develops. (a) Normalized pressure fluctuations (curves are shifted by ±0.01 in the vertical axes for a better representation). The mean values are 283, 261 and 88 bar for T1, T2 and T3, respectively. The subscript Ti represents the different transducers. (b) the respective Fourier transform for T1 showing the fast fluctuation of 28 Hz and the small amplitude (around 0.01 bar) for this instability.

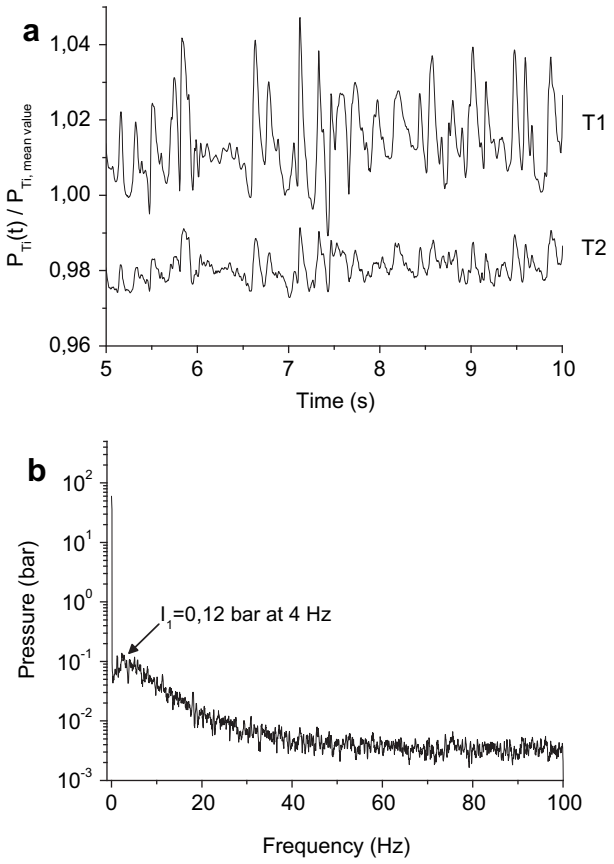

Fig. 9. Pressure fluctuations and related spectra for PE-LCB sample at a shear rate of 787 s^{-1} where the gross melt fracture instability develops. (a) Normalized pressure fluctuations (curves are shifted in the vertical axes for a better representation). The mean values of the pressure are 181 bar for T1 and 149 bar for T2. The subscript Ti represents the different transducers. (b) The respective Fourier transform for T1.

studied. Independently of the conditions, this instability is characterized by a less regular behavior than that associated with PE-L, explaining the characteristic broad peak found in the Fourier analysis. At some shear rates, it was possible to detect two peaks simultaneously. The related frequencies are not multiples of each other therefore the second peak is not a higher harmonic from the same instability and probably it is related with another instability occurring at the same time inside the barrel. The cross-correlation function between the transducers show a drastic decrease in the beginning reaching a non-zero but oscillatory values already after around 0.1 s at a shear rate of 787 s^{-1}. This means that the signals are basically not correlated at short times. The different behavior between PE-L and PE-LCB under gross melt fracture conditions could be associated with the higher elasticity in melt state of PE-L that explains its plug-flow fluctuations (see G' values in Fig. 3).

The spurt instability has been related with the presence of long-chain branching in polyethylenes [39]. It seems nevertheless that there is a critical value for the degree of long-chain branching. Above this threshold the polymer does not develop this instability as PE-LCB has much higher amount of long-chain branching (3 LCB/1000 CH_2) than the samples used in reference 39 (less than 1 LCB/1000 CH_2).

4.3. Effect of short chain branching

Fig. 10 shows the normalized pressure oscillations for the PE-7SCB sample at a shear rate of 315 s^{-1} together with the respective Fourier analysis for the T2 signal. Under these conditions PE-7SCB develops the sharkskin instability as a surface distortion appears in the extrudate. Therefore the slope changes in the flow curve (Fig. 4) for this sample is due to the beginning of the sharkskin instability associated with the presence of short chain branching in the polymer [49]. Noteworthy, the three transducers located inside the slit-die are able to detect pressure oscillations. To the best of our knowledge, the last finding is unique and it shows the high sensitivity of this new set-up. The normalized pressure fluctuations are higher as the polymer passes through the die, therefore:

$$\left(\frac{I_1}{I_0}\right)_{T3} > \left(\frac{I_1}{I_0}\right)_{T2} > \left(\frac{I_1}{I_0}\right)_{T1}$$

This is due to the decrease in the mean pressure value because of the energy loss by frictional forces (see for example the Hagen–Poiseuille equation). The pressure fluctuations are around 0.05% with respect to the mean value. Comparing the pressure fluctuations arising from sharkskin instability with those coming from the spurt instability (around 10%), a clear dependency of the relative pressure fluctuation with the kind of instability is observed. The pressure fluctuations under sharkskin condition are closer to those associated with gross melt fracture. The peak related with the Fourier analysis has a frequency of 22 Hz (Fig. 10) and from the characteristic length of the extrudate is possible to estimate its characteristic frequency at around 60 Hz. The difference in the frequencies is, as already mentioned, associated with changes as the polymer goes from melt-state with a lamellar shear-flow inside the die to solid-state with a plug flow outside the die. These differences in frequencies could decrease depending of the shear rate. The PE-13SCB sample presents the same behavior than PE-7SCB.The pressure fluctuations are not shown here.

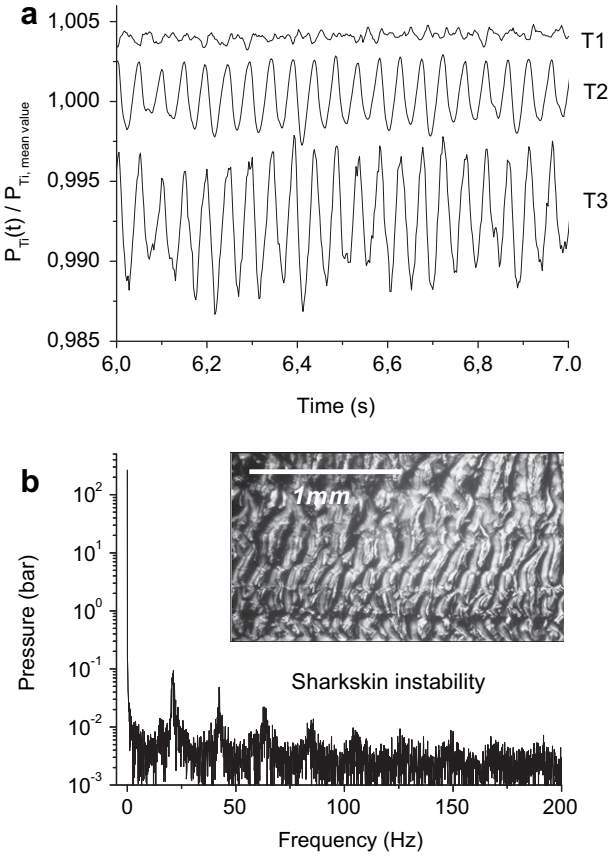

Fig. 10. (a) Normalized pressure fluctuations for PE-7SCB sample at a shear rate of 315 s^{-1} (curves are shifted for simplicity). The mean values of the pressure are 341 bar for T1, 263 bar for T2, and 41 bar for T3. (b) The respective Fourier transform for T2.

The use of our new methodology, consisting of a unique high sensitivity pressure detection together with the application of an advanced mathematical framework, allowed measuring directly inside the die, both the amplitude and the frequency of pressure fluctuations arising from sharkskin instability. To the best of our knowledge the special features of our device and mathematical analysis allowed, for the first time, an accurate and in-situ characterization of the pressure fluctuations arising from sharkskin. Such analysis was not possible until now and it was not reported by other researchers, mainly due to experimental limitations of the equipment available. The nature of the pressure fluctuations associated with sharkskin (low pressure deviations and very fast frequencies) requires setups with very high pressure resolution (ΔP of around 5×10^{-3} bar) and extremely high acquisition rates (3×10^4 s^{-1}). These values are unique and characteristic of our novel set-up. In addition, T3 gives the highest relative pressure fluctuations, showing that it is substantially easier to detect the fluctuations in areas close to the die exit. Our results are therefore not in contradiction with previous ones.

These new findings can be related with the origin of the sharkskin instability [26]. The pressure fluctuations detected inside the die can be caused by: (1) the constitutive nature of the sharkskin producing pressure oscillations inside the die [9,11–17]; or (2) upstream propagation with the speed of sound of processes that occurs in the die-exit, therefore faster than the time resolution of the cross-correlation between our transducers due to the 10 μs time resolution of the raw data. Theories that stress the origin of the sharkskin in the die-exit are supported by the elimination of this instability by changing the surface condition of the die [51,53–57]. For example, the presence of the Dynamar-coating forces the polymers to slip, decreasing the stress in the exit due to the reduction in the extensional flow. The change in the surface introduce a soft transition from a slip to a free plug flow in the extrudate and it reduces the stress in the whole die [11,13]. The presence of the slip area nevertheless could eliminate or reduce pressure oscillations originating upstream. Eq. (11) states that the

pressure decreases when the fluid increases its velocity, therefore the slippery surface could not avoid the origin of the instability but it could reduce its effect (see for example Ref. [58]). One example of the last phenomena is given by Barone et al. [59]. They made an artificial surface discontinuity inside the die covering its upper half-part with a slippery surface. Although at the border between the slippery surface and the normal-surface a pressure oscillation develops, no instability in the extrudate was observed. The Bernoulli equation also explains why the slippery surface eliminates (or postpone to higher shear rates) not only the sharkskin but also gross melt instabilities [51].

Analyzing the cross-correlation function (Eq. (10)) for T1–T2, a maximum at a time that is close to a half-period of the instability is observed. For T2–T3 the maximum is found at a zero-time-lag. The last shows a different behavior with respect to the spurt and gross melt fracture instabilities. Moreover, the non-zero-time-lag between T1 and T2 allows us to reject the hypothesis that the pressure fluctuations detected inside the die are due to a back-propagation of processes coming from the die-exit. In this case, as the propagation would have the velocity of the sound, our system will not be able to detect it and a close to zero-time-lag must appear; that is not our case. The rejection of this hypothesis is confirmed by the absolute pressure fluctuations along the die as they have not the decreasing tendency upstream the die-exit expected for a back propagation through an elastic media. The correlation between T2 and T3 could indicate that the sharkskin instability has a cooperative dynamic in areas close to the exit. Probably a fluctuating plug flow is developed that would explain the zero-time-lag between T2 and T3 for the sharkskin effect. Analyzing the theoretical results based on a constitutive approach of Shore et al. a similar tendency is seen [60]. In particular, they show that in the die-exit area an elastic oscillation could occur under a condition of a distribution of stresses inside the die. Finally, to reject the idea that this maximum at zero-time-lag is an artifact related with a Nyquist frequency [45], we also measured the cross-correlation function at different shear rates where the sample develops sharkskin, and the same vanishing time-lag was found.

Under the hypothesis of the constitutive nature of the sharkskin instability, it is possible that the pressure fluctuations coming from inside the die undergo an amplification process as they approach the die-exit due to the hydrodynamic singularity at the die-exit. This amplification can produce the melt fracture (or coil–stretch transition), that explain the periodicity of this instability. The last is supported by numerical simulations that show that polymers that develop sharkskin instability in the die-exit need a pre-stretching condition from some area upstream [13,14]. Therefore, the constitutive pressure oscillations coming from the die could fit this condition.

Based on the above mentioned, it can be assumed that the pressure oscillations already detected inside the die are new evidences towards the constitutive origin of the sharkskin instability.

4.4. Effect of the shear rate and polymer topology

Figs. 11 and 12 summarize the effect of both topology and shear rate on the characteristic frequency and the relative pressure fluctuation (measured by the I_1/I_0 parameter in percentage, see Section 3 and Eqs. (7) and (8)) of the instabilities, respectively. There is a strong effect of the polymer topology and the shear rate on the instability and differences of several orders of magnitude are detected between the PE samples. In particular, the high-density polyethylene (PE-L) develops the spurt instability at low shear rates (between 140 and 400 s^{-1}). These instabilities are characterized by low frequencies between 0.01 and 0.1 Hz (roughness/smooth period in the extrudate) and high I_1/I_0 values (around 10%). The PE-L sample also presents a second kind of spurt instability at shear rates around

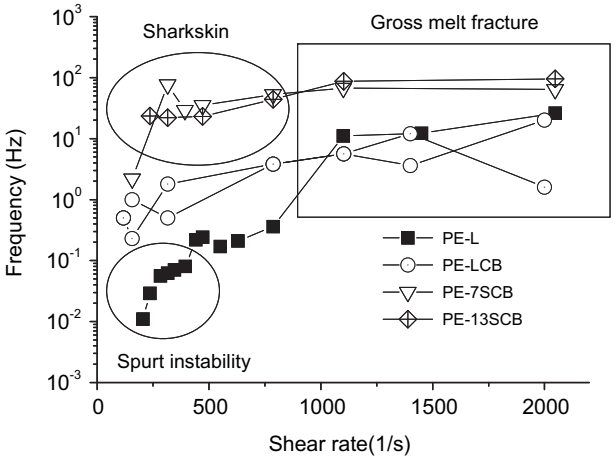

Fig. 11. Effect of the shear rate on the characteristic frequency of the melt instability for polymers with different topologies.

600 s^{-1} associated with an increase in the I_1/I_0 parameter, together with a small jump in the characteristic frequency, which has been reported previously for other polyethylenes as due to a cohesive breakdown [17,51]. At shear-rates higher than 800 s^{-1}, the sample displays a gross melt fracture (see next sections for details) with high characteristic frequencies (>10 Hz) and low relative pressure fluctuations between 0.01 and 0.1%. If the amount of long-chain-branching increases, as in sample PE-LCB, the spurt instability is not observed and gross melt fracture is developed in the whole shear rate range studied. The gross melt fracture develops with frequencies between 0.1 and 10 Hz and I_1/I_0 values around 0.1%. The frequencies for the oscillations of PE-L and PE-LCB samples converge at high shear rate, although the same is not observed for the relative pressure fluctuation determined via the I_1/I_0 values. We conclude that the pressure oscillation of the gross melt fracture is controlled by the presence of long-chain branching.

Samples with short chain branching (PE-7SCB and PE-13SCB) present sharkskin instabilities at shear rates between 100 and 800 s^{-1} as a surface distortion appears on the extrudate, which is characterized by high frequencies (between 10 and 100 Hz) and low I_1/I_0 values (around 0.01%). The main characteristics of the sharkskin are not affected by the amount of short chain branching as these samples have almost the same values in these properties.

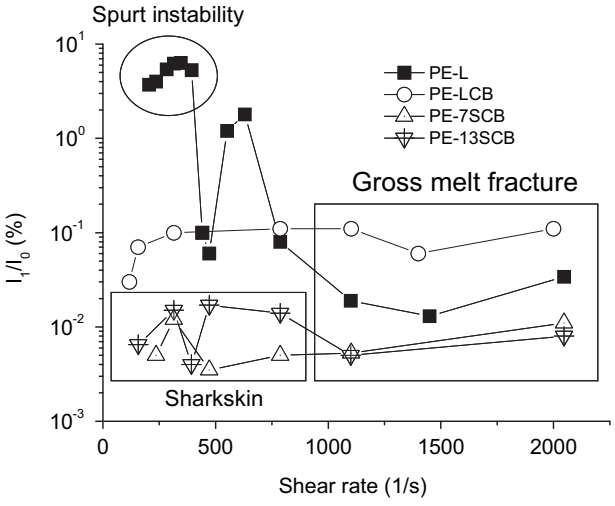

Fig. 12. Effect of the shear rate on the I_1/I_0 values of the melt instability for polymers with different topologies.

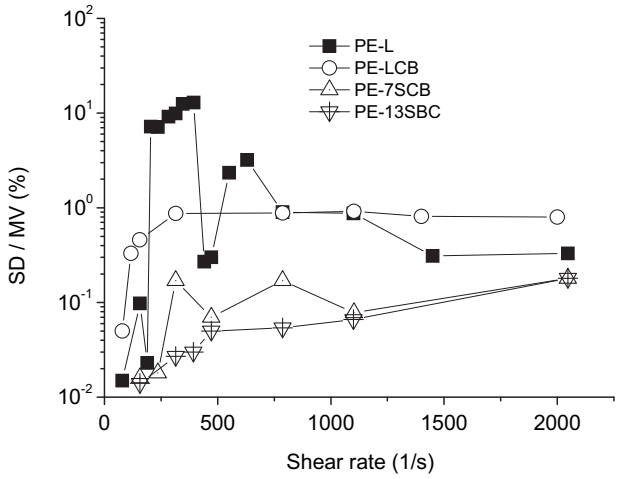

Fig. 13. Effect of the shear rate on the relative pressure fluctuation measured as the ratio between the standard deviation of the pressure signal (SD) and its mean value (MV), in melt instabilities of polymers with different topologies.

At shear rates higher than 800 s^{-1} these samples develop gross melt fracture instabilities. The peak in the Fourier spectra under these conditions is related with the bulk instability and not with the sharkskin. Although sharkskin and gross melt fracture are different phenomena, they present the same order of magnitude for both the characteristic frequency and the I_1/I_0 values, and they are not affected significantly by the shear rate in the range studied. A possible route to differentiate both instabilities is, as stated above, by analyzing the correlation functions (Eqs. (9) and (10)).

To compare our novel approach with the moment analysis, Fig. 13 presents the effect of the shear rate and polymer topology on the relative pressure fluctuations as measured by the ratio between the standard deviation of the pressure signals (square root of the second moment) and its mean value (first moment around zero). The same tendency is found when these data are compared with those from Fig. 12, although the data coming from the moment analysis are higher than the data measured by FT and do not contain any information about the related time scale.

From Figs. 11 and 12 it is concluded that by means of our new device all potential instabilities can be detected. The polymer structure (e.g. Mn, Mw, topology, branch number and branch length) has an important effect on the specific instability that is developed. In the case of the gross melt fracture (that is common in all the samples), its frequency and relative pressure fluctuation depend of the microstructure of the polyethylene, as different samples have different values at high shear rates. A summary of the relation between polymer topology and melt instability properties is shown in Table 2.

It is important to stress that the I_1/I_0 parameter is a normalized property based on the pressure fluctuation. Therefore, when the absolute pressure fluctuation increases proportional to its mean value ($I_1 \propto I_0$), this parameter will not be shear-rate dependent, as it is sometime observed in Fig. 12. Similar behavior could occur with the characteristic frequency of the fluctuation, as it is defined as the ratio between the extrudate velocity and the characteristic length of the instability (λ). When λ is proportional to the extrudate velocity, the characteristic frequency will not be shear-rate dependent neither.

Fig. 14 displays on a log–log plot the relation between the shear stress (σ_{zx}) and the characteristic frequency ($\omega_1/2\pi$) for sharkskin and gross melt fracture instabilities, for all investigated samples. A linear relationship is observed, indicating that the frequency of the instability is related with the shear stress, independent of the polymer topology. It is highlighted that the relation is:

$$\omega_1 = m\sigma_{zx}^{3.4} \tag{15}$$

where m represents a constant with a current value $\approx 10^{-18}$. The exponent 3.4 is similar to the found in the relationship between the molecular weight of a polymer and its viscosity due to the presence of entanglements [61]. No common tendency is found for the shear stress against I_1/I_0, supporting the finding that the relative amplitude of the pressure fluctuations depends on the polymer topology.

4.5. Effect of the die-entrance angle

Changing the die-entrance angle from 180° to 60° more information about the spatial origin of the melt instabilities is expected. For the PE-L sample, decreasing the angle eliminates (or postpone) the melt instability that occurs at 2047 s^{-1}. Using an angle of 60° a smooth surface appears in the extrudate instead of the characteristic wavy distortion occurring with the angle of 180°. The dependence with the die-entrance angle means that this instability is due to turbulences in the barrel at areas close to the entrance of the die, confirming that it is gross melt fracture. A similar phenomenon is found under spurt conditions. As it was shown above, using the die-entrance angle of 180°, the extrudate presents the two characteristic areas of the spurt instability. In one of this area the polymer shows a wavy distortion related with the slip process, and in the other its surface is smooth due to the stick condition. By using an angle of 60° only a change in the diameter of the polymer is detected during the spurt instability and there is no any evidence of distortions even under slip conditions. The last means that the wavy distortion in the extrudate under spurt instability using a die-entrance angle of 180° is related with the increase in the velocity (slip condition in the die) that generates

Table 2
Relation between polymer topology and its melt instability properties.

Topology	Melt instability	Characteristic frequency Hz	Relative pressure fluctuation I_1/I_0 [%]
Linear	Spurt	10^{-2}–10^{-1}	10^{0}–10^{1}
	Gross melt fracture	10^{1}–10^{2}	10^{-2}–10^{-1}
Long chain branching	Gross melt fracture	10^{0}–10^{2}	10^{-2}–10^{0}
Short chain branching	Sharkskin	10^{0}–10^{2}	10^{-3}–10^{-1}
	Gross melt fracture	10^{1}–10^{2}	10^{-3}–10^{-1}

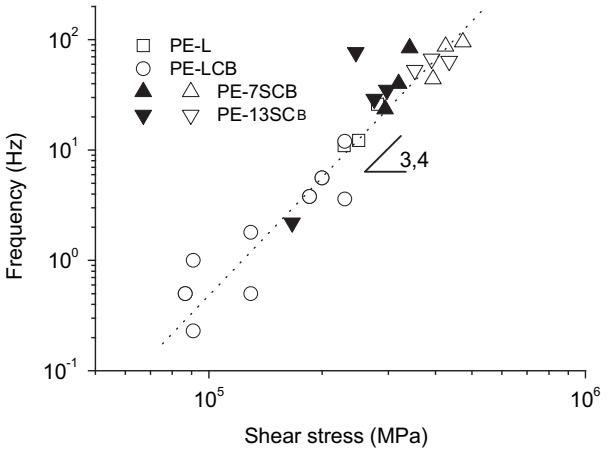

Fig. 14. Effect of the shear stress on the characteristic frequency of both gross melt fracture and sharkskin instabilities. Filled-symbols are related with sharkskin instability and the open-symbols representing the gross melt fracture instability. The dotted line according to Eq. (15): $m = 10^{-8}$ and $\sigma = 3.4$.

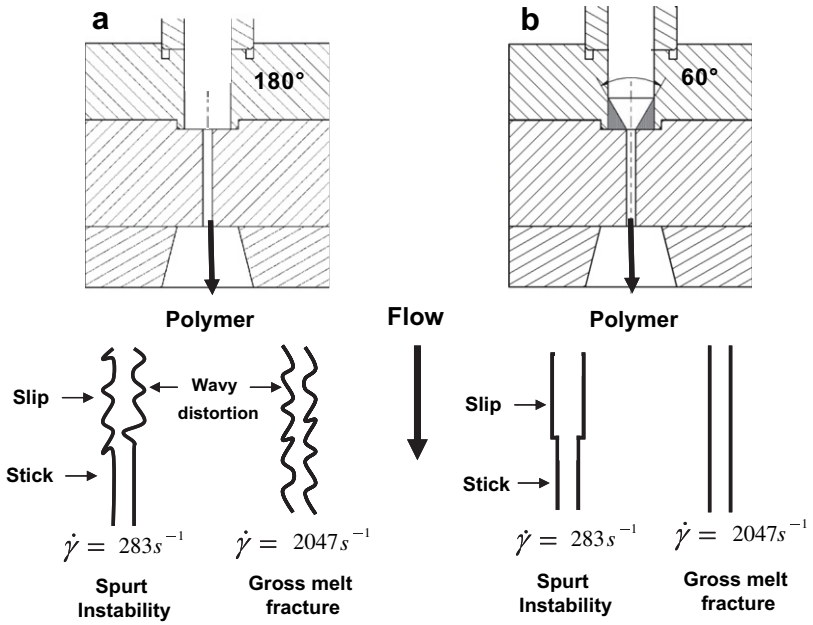

Fig. 15. Effect of the angle of the die-entrance on both spurt instability and gross melt fracture instabilities. (a) Entrance-angle of 180°. The polymer develops gross melt fracture at high shear rates and in the spurt instability under the slip condition is observed a wavy distortion in the extrudate due to the increase in the velocity. (b) Entrance-angle of 60°. The gross melt fracture is erased (or postponed) toward high shear rates and in the spurt instability only an increase in the diameter is observed when the slip process appears.

gross melt fracture. Similar results were reported by Wang et al. [17]. The effect of the die-entrance angle is summarized in Fig. 15.

At a shear rate of 315 s^{-1} the PE-7SCB sample does not show any significant difference in its surface instability when the two die-entrances are used, supporting that the instability that is developed under these conditions is sharkskin. Therefore, we would rule out other possible mechanisms that could explain the pressure oscillation detected for this sample with our set-up under these conditions.

5. Conclusions and outlook

By means of high sensitive pressure transducers located inside a slit-die the effect of the polymer topology and the shear rate on the main characteristics of melt flow instabilities were in-situ measured in a capillary rheometer. An advanced mathematical framework is presented and applied to process the experimental data allowing a substantial improvement by a factor of 10^3 and 10^2 in terms of time (typically 1 ms) and pressure (typically 5 mbar) resolutions compared with a conventional set-up. These improvements allow to characterize for the first time the whole range of melt instabilities in-situ. The characteristic frequency and the relative pressure fluctuation of the instabilities together with the time cross-correlation function for the data from the different transducers were analyzed.

The sample with low amount of long-chain branching develops spurt instability which is characterized by low frequencies (around 0.05 Hz) and high relative pressure fluctuations (around 10%) as measured by the I_1/I_0 parameter (see Eq. (8)). It was additionally observed that this instability starts in a region inside the die and it propagates along it. The cross-correlation function allows us to estimate the velocity of this propagation and it is found that accelerates along the die as an "avalanche". Increasing the amount of long-chain branching, the spurt instability disappears and the gross melt fracture is observed in the whole range of shear rates studied. In general, this instability has higher frequencies (between 1 and 30 Hz) and lower I_1/I_0 values (between 0.1 and 0.05%) than spurt instabiltiy. In sample with high content of long-chain branching the gross melt fracture instability becomes less regular than in the linear polymer. The sharkskin instability develops in samples with short-chain branching and it is characterized by high frequencies (between 10 and 100 Hz) together with low I_1/I_0 values (around 0.01%). Our results open up the idea that this instability has its origin inside the die and not only at the die-exit, and it gives new evidence towards a possible constitutive origin. Plotting the shear stress against the characteristic frequency for all the samples, a power law relationship is found for gross melt fracture and sharkskin instabilities. Nevertheless, a common tendency is not found when the shear stress is plotted against the I_1/I_0 values.

Our novel approach will allow the development of an "intelligent" extruder able to detect automatically the onset of melt instabilities. Under this new concept, the extruder itself will conduct the changes in the operational variables that would avoid these distortions increasing the throughput and lowering at the same time energy consumptions.

Acknowledgments

The authors gratefully acknowledge the financial support of CONICYT, project FONDECYT INICIACION EN INVESTIGACION 11075001, and the support of the Alexander von Humboldt Foundation. An acknowledgment is due to the work undertaken by Alfons Becker, during the development and validation of the melt flow instabilities prototype. We would also like to thank the Göttfert GmbH, specifically to Dr. J. Sunder and Dr. A. Göttfert, for making our ideas and set-up commercially available. Dr. I. Vittorias is greatly acknowledged for supplying some of the materials analysed within this work.

References

[1] Larson RG. Rheol Acta 1992;31:213–63.
[2] Denn MM. Annu Rev Fluid Mech 2001;33:265–87.

[3] El Kissi N, Piau JM. J Rheol 1994;38:1447–63.
[4] Wang SQ. Adv Polym Sci 1999;138:227–75.
[5] Hill DA, Hasegawa T, Denn MM. J Rheol 1990;34:891–918.
[6] Wang SQ, Drda P. Macromolecules 1996;29:2627–32.
[7] Legrand F, Piau JM. J Non-Newtonian Fluid Mech 1998;77:123–50.
[8] Tao Z, Huang JC. J Appl Polym Sci 2005;98:903–11.
[9] Migler KB, Qiao F, Flynn K. J Rheol 2002;42:383–400.
[10] Mackley MR, Rutgers RPG, Gilbert DG. J Non-Newtonian Fluid Mech 1998;76: 281–97.
[11] Rutgers RPG, Mackley MR. J Non-Newtonian Fluid Mech 2001;98:185–99.
[12] Rutgers R, Mackley M. J Rheol 2000;44:1319–34.
[13] Arda DR, Mackley MR. J Non-Newtonian Fluid Mech 2005;126:47–61.
[14] Venet C, Vergnes B. J Non-Newtonian Fluid Mech 2000;93:117–32.
[15] Cogswell FN. J Non-Newtonian Fluid Mech 1977;2:37–44.
[16] Barone JR, Plucktaveesak N, Wang SQ. J Rheol 1998;42:813–32.
[17] Wang SQ, Drda P. Macromol Chem Phys 1997;198:673–701.
[18] El Kissi N, Piau JM, Toussaint F. J Non-Newtonian Fluid Mech 1997;68:271–90.
[19] Barone JR, Wang SQ. J Rheol 2001;45:49–60.
[20] Deeprasertkul C, Rosenblatt C, Wang SQ. Macromol Chem Phys 1998;199: 2113–8.
[21] Fernandez M, Vega JF, Santamaria A, Muñoz-Escalona A, Lafuente P. Macromol Rapid Commun 2000;21:973–8.
[22] Shore JD, Ronis D, Piche L, Grant M. Phys Rev Lett 1996;77:655–8.
[23] Moleenar J, Koopmans RJ, den Doelder CFJ. P R Enferm 1998;58:4683–91.
[24] Bertola V, Meulenbroek B, Wagner C, Storn C, Morozov A, van Saarloos W, et al. Phys Rev Lett 2003;90:114502.
[25] Meulenbroek B, Storm C, Bertola V, Wagner C, Bonn D, van Saarloos W. Phys Rev Lett 2003;90:024502.
[26] Palza H, Naue IFC, Wilhelm M. Macromol Rap Comm 2009;30:1799–804.
[27] Boukany PE, Tapadia T, Wang SQ. J Rheol 2006;50:641–54.
[28] Lim FJ, Schowalter WR. J Rheol 1989;33:1359–82.
[29] Leger L, Hervet H, Massey G, Durliat E. J Phys Condens Matter 1997;9:7719–40.
[30] Migler KB, Hervet H, Leger L. Phys Rev Lett 1993;70:287–90.
[31] Münstedt H, Schmidt M, Wassner E. J Rheol 2000;44:413–27.
[32] Brochard F, de Gennes PG. Langmuir 1992;8:3033–7.
[33] Wang SQ, Drda P. Macromolecules 1996;29:4115–9.
[34] Hatzikiriakos SG, Dealy LM. J Rheol 1992;36:845–84.
[35] Den Doelder CFJ, Koopmans RJ, Molenaar J. J Non-Newtonian Fluid Mech. 1998;79:503–14.
[36] Molenaar J, Koopmans RJ. J Rheol 1994;38:99–109.
[37] Aarts ACT, van deVen AAF. Continuum Mech Thermodyn 1999;11:113–39.
[38] Den Doelder CFJ, Koopmans RJ, Molenaar J, van de Ven AAF. J Non-Newtonian Fluid Mech 1998;75:25–41.
[39] Filipe S, Vittorias I, Wilhelm M. Macromol Mater Eng 2008;293:57–65.
[40] Filipe S, Becker A, Barroso V, Wilhelm M. App Rheol 2009;19:23345.
[41] van Dussschoten D, Wilhelm M. Rheol Acta 2001;40:395–9.
[42] Wilhelm M. Macromol Math Eng 2002;287:83–105.
[43] Wilhelm M, Reinheimer P, Ortseifer M. Rheol Acta 1999;38:349–56.
[44] Hilliou L, van Dusschoten M, Wilhelm M, Burhin H, Rodger ER. Rubber Chem Technol 2004;77:192–9.
[45] Honerkamp J. Stochastic dynamical systems: concepts, numerical methods, data analysis. New York: VCH; 1994.
[46] Abarbanel HDI. Rev Mod Phys 1993;65:1331–40.
[47] Wood-Adams P, Dealy JM, de Groot AW, Redwine OD. Macromolecules 2000; 33:7489–99.
[48] Venet C, Vergnes B. J Rheol 1997;41:873–92.
[49] Yamaguchi M, Miyata H, Tan V, Gogos C. Polymer 2002;43:5249–55.
[50] Allal A, Lavernhe A, Vergnes B, Marin G. J Non-Newtonian Fluid Mech 2006; 134:127–35.
[51] Piau JM, El Kissi N, Toussant F, Mezghani A. Rheol Acta 1995;34:40–57.
[52] Bird RB, Armstrong RC, Hassager O. Dynamics of polymeric liquids, fluid dynamics. 2nd ed., vol. 1. New York: Wiley; 1987.
[53] Moynihan RH, Baird DG, Ramanathan R. J Non-Newtonian Fluid Mech 1990;36:255–63.
[54] Wang SQ, Drda P, Inn YW. J Rheology 1996;40:875–98.
[55] Migler KB, Lavallee C, Dillon MP, Wood SS, Gettinger CL. J Rheol 2001;45:565–81.
[56] Ghanta VG, Riise BL, Denn MM. J Rheol 1997;43:435–42.
[57] Ramamurthy AV. J Rheol 1986;30:337–57.
[58] Hong Y, Coombs SJ, Cooper-White JJ, Mackay ME, Hawker CJ, Malmstrom E, et al. Polymer 2000;41:7705–13.
[59] Barone J, Wang SQ. Rheol Acta 1999;38:404–14.
[60] Shore JD, Ronis D, Pichè L, Grant M. Phys Rev E 1997;55:2976–92.
[61] Doi M, Edwards SF. The theory of polymer dynamics. Oxford Science Publications; 1986.